

Identification of a paramagnetic recombination center in silicon/silicon-dioxide interface

T. Matsuoka, L. S. Vlasenko, M. P. Vlasenko, T. Sekiguchi, and K. M. Itoh

Citation: *Appl. Phys. Lett.* **100**, 152107 (2012); doi: 10.1063/1.3702785

View online: <http://dx.doi.org/10.1063/1.3702785>

View Table of Contents: <http://apl.aip.org/resource/1/APPLAB/v100/i15>

Published by the [American Institute of Physics](#).

Related Articles

Magneto-mechanical resonance of a single superparamagnetic microbead trapped by a magnetic domain wall
J. Appl. Phys. **111**, 07B310 (2012)

Dynamics of superparamagnetic microbead transport along magnetic nanotracks by magnetic domain walls
Appl. Phys. Lett. **100**, 082401 (2012)

Note on de Haas-van Alphen diamagnetism in thin, free-electron films
AIP Advances **2**, 012105 (2012)

Irradiation enhanced paramagnetism on graphene nanoflakes
Appl. Phys. Lett. **99**, 102504 (2011)

Nonlinear stationary ac response of the magnetization of uniaxial superparamagnetic nanoparticles
J. Appl. Phys. **110**, 023901 (2011)

Additional information on *Appl. Phys. Lett.*

Journal Homepage: <http://apl.aip.org/>

Journal Information: http://apl.aip.org/about/about_the_journal

Top downloads: http://apl.aip.org/features/most_downloaded

Information for Authors: <http://apl.aip.org/authors>

ADVERTISEMENT



HAVE YOU HEARD?

Employers hiring scientists
and engineers trust
physicstodayJOBS



<http://careers.physicstoday.org/post.cfm>

Identification of a paramagnetic recombination center in silicon/silicon-dioxide interface

T. Matsuoka,¹ L. S. Vlasenko,² M. P. Vlasenko,² T. Sekiguchi,¹ and K. M. Itoh^{1,a)}

¹*School of Fundamental Science and Technology, Keio University, Yokohama 223-8522, Japan*

²*A. F. Ioffe Physico-Technical Institute, 194021 St. Petersburg, Russia*

(Received 25 January 2012; accepted 25 March 2012; published online 11 April 2012)

A paramagnetic recombination center having an orthorhombic symmetry with $g[110] = 2.0095(2)$, $g[001] = 2.0038(2)$, and $g[\bar{1}10] = 2.0029(2)$ is found at the interface between silicon and native oxide. The center is referred to P_m center and observed by a spin dependent recombination based electron paramagnetic resonance detection that has the sensitivity of $\sim 10^{11}$ spins/cm². The employment of an isotopically enriched ²⁸Si sample with the concentration of ²⁹Si nuclear spins reduced to 0.017% leads to narrowing of the resonance line. This narrowing is the key for the accurate determination of the angular dependence of the g-factor. © 2012 American Institute of Physics. [<http://dx.doi.org/10.1063/1.3702785>]

A variety of defects situating at the interfaces between silicon and oxide films have been studied extensively in the past 40 years since they affect strongly the device performance of the metal-oxide-silicon field effect transistor (MOS-FET).¹ In 1971, dangling bond defects (P_b -centers) were found at the interface,² and they were classified into several different types: P_b for (111) and (110) interfaces and P_{b0} and P_{b1} for (100) interfaces.³⁻⁵ These discoveries have stimulated experimental studies to identify structures, energy levels, and densities of the interface defects,⁶⁻¹⁴ and theoretical calculations on the microscopic structures of the interface and defects.¹⁵⁻¹⁸ In addition, E' -center produced by irradiation and other defects involving nitrogen, phosphorous, and boron have been identified at the interface.⁷ Many of these interface defects were observed by electron paramagnetic resonance (EPR) spectroscopy. Moreover, such defects very often act as recombination centers for electrons and holes making them observable by a special EPR technique utilizing highly sensitive spin-dependent-recombination (SDR) based detection.¹⁹⁻²³ Here, the change in the microwave photoconductivity of the sample induced by the change in the recombination rate of the carriers under magnetic resonance is detected. Since SDR-EPR method has higher sensitivity (10^{11} cm⁻² spin density) than the conventional EPR, it has been used for detection of defects that cannot be observed by the conventional EPR.¹ The main focus of the EPR characterization is the measurement of the angular dependence of the line position, i.e., g-factor, to reveal the microstructure of the defect. Moreover, the EPR linewidth is determined by the local environment around the defect. The previously reported EPR spectra of Si/SiO₂ interface defects have close values of g-factors ($g \sim 2$) and broad overlapping EPR lines. This prevents the accurate measurement of the angular dependence of the g-factors. One of the major sources of the line broadening is the random magnetic field induced by the random distribution of ²⁹Si nuclear spins. Natural silicon is composed of three isotopes, ²⁸Si (92.23%), ²⁹Si (4.67%), and ³⁰Si (3.10%), and only ²⁹Si has a non-zero

nuclear spin $I = 1/2$. Hyperfine interaction between electrons and ²⁹Si nuclear spins causes significant inhomogeneous broadening of the EPR linewidths.²⁴⁻²⁶ The present work shows that the EPR linewidths of the interface defects are decreased by isotopic enrichment of Si crystals by the nuclear spin-free ²⁸Si stable isotope. The narrowing of the EPR lines allows us to resolve EPR spectra and to analyze the angular dependences of the g-factor of the center.

A sample used for the experiments was a n-type phosphorus-doped ($[P] \approx 10^{15}$ cm⁻³) float-zone (FZ) ²⁸Si-enriched silicon with the concentration of ²⁹Si reduced to 0.017%. As a reference sample, natural silicon with the concentration of ²⁹Si (4.67%) having the same phosphorus concentration was prepared. Hereafter, we refer to these samples as ²⁸Si and ^{nat}Si. A typical size of the sample for EPR was $10 \times 3.5 \times 1$ mm³ with 10×3.5 mm² surface being (110) plane and 10×1 mm² being (100). Oxide films were produced by two kinds of oxidation: native oxidation in air at room temperature and dry thermal oxidation in oxygen atmosphere (800 °C, 1 h). The thicknesses of oxide films measured by the ellipsometer were 1.8 nm and 8.9 nm for the native and thermal oxides, respectively. Prior to the oxidation, the sample was etched in 1:3 mixture of hydrofluoric and nitric acids for few seconds followed by treatment in 5% aqueous solution of hydrofluoric acid for 1 min to produce hydrogen terminated surfaces. Conventional EPR measurements were performed by the X-band spectrometer (JEOL JES-RE3X) with a cylindrical TE₀₁₁-mode cavity and the externally applied magnetic field modulated by 100 kHz. The same EPR spectrometer was used for the SDR-EPR measurements in which the steady-state microwave photoconductivity of the sample by irradiation of the band-edge light (100 W halogen lamp) was obtained at the start.²⁰⁻²² Then saturation of an EPR transition between target magnetic sublevels was achieved by the microwave excitation (20 mW) followed by the measurement of the reduction in the photoconductivity of the sample when the swept magnetic field meets the EPR condition to enhance the electron-hole recombination. No electrical contacts to the sample were needed since the change of the photoconductivity was monitored as the change of the microwave absorption in the

^{a)}Author to whom correspondence should be addressed. Electronic mail: kitoh@appi.keio.ac.jp.

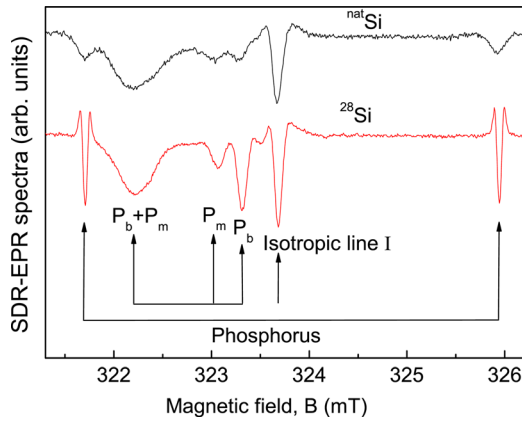


FIG. 1. SDR-EPR spectra for ^{nat}Si and ^{28}Si samples recorded at 16 K with $B \parallel [111]$. The samples were measured after native oxide formation at room temperature in air for 17 days.

cavity. The Q-factor of the cavity dropped by 20% under illumination because of absorption of the electrical component of the microwave field by the photoexcited carriers and further when the recombination was enhanced by the magnetic resonance. The temperature of the sample was varied in the range of 10–35 K using the helium gas flow cryostat (Oxford Instruments ESR900). To suppress the strong broad background due to the change in the sample magnetoresistance, the second derivative of the EPR lines was recorded. The magnetic field at the sample was calibrated by the well-known phosphorus EPR lines (g -factor ~ 1.99850 and hyperfine constant $A \sim 117.53$ MHz)²⁷ arising from the sample in the same measurement.

SDR-EPR spectra detected in ^{28}Si and ^{nat}Si samples with native oxide films are shown in Fig. 1. Here, electron paramagnetic resonance lines of phosphorus, P_b , isotropic line labeled I, and previously not reported P_m are seen. The isotropic line I has similar line position with NL15 which is one of shallow thermal donor (STD) signals that shows cubic symmetry.²⁸ These lines are detectable at the temperature ranges of 10–35, 10–24, and 14–35 K for P_b , I, and P_m , respectively. The conventional EPR measurements on the same samples show only the phosphorus signals with no signs of P_b , I, and P_m . Each line in Fig. 1 was fitted by second-derivative line shapes of Lorentzian or Gaussian to determine the linewidth. The Lorentzian fitted better with peaks of P_b , I, and P_m , while Gaussian fitted better with lines of phosphorus. The resulting linewidths yielded by the respective fittings are shown in Table I. The narrowing of lines by the depletion of ^{29}Si nuclear spins is observed for all lines. The ratio of linewidths detected in the ^{nat}Si sample to that in the ^{28}Si sample is as large as four for phosphorus but smaller than two for P_b , I, and P_m . The linewidths of P_b , I,

TABLE I. Linewidths of the SDR-EPR signals.

Samples	Linewidth [mT]			
	Phosphorus	P_b	I	P_m
^{nat}Si	0.26(1)	0.35(2)	0.168(3)	0.29(3)
^{28}Si	0.062(1)	0.19(1)	0.13(1)	0.20(2)
$^{nat}\text{Si}/^{28}\text{Si}$ linewidth ratios	4.2(2)	1.8(1)	1.3(1)	1.4(2)

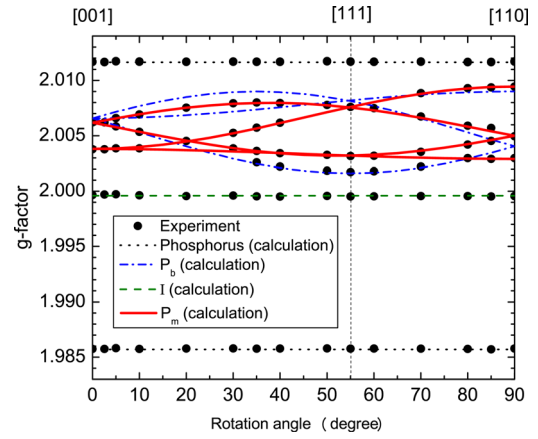


FIG. 2. Angular dependences of the g -factors of SDR-EPR spectra detected in ^{28}Si sample rotated around $[1\bar{1}0]$ crystal axis. The experimental points (\bullet) are compared with calculation based on previously reported spin Hamiltonian parameters for phosphorus (dotted line)²⁷ and P_b (broken curves).¹² The dashed line and the solid curves are calculated g -factor components for I ($g = 1.9996(2)$) and P_m , respectively.

and P_m may have been broadened by other contributions such as inhomogeneous deformation arising from the silicon/silicon-dioxide interface.

The angular dependences of the g -factors for the SDR-EPR spectra in ^{28}Si sample are shown in Fig. 2. The narrowing of the lines in ^{28}Si sample allows us to separate the P_m lines from others. P_m spectrum shows an orthorhombic symmetry with $g[110] = 2.0095(2)$, $g[001] = 2.0038(2)$, and $g[\bar{1}10] = 2.0029(2)$. These values are close to the g -tensor components of Si-B1 EPR spectrum originating from the negatively charged A-center (oxygen + vacancy complex) having $g[110] = 2.0096$, $g[001] = 2.0029$, and $g[\bar{1}10] = 2.0019$.²⁹ However, we argue that P_m spectrum is not Si-B1 because the SDR-EPR spectrum shows no Si-SL1 lines.^{30–32} Si-SL1 spectrum originates from the photoexcited triplet paramagnetic state of A-center, which we should have been observed in our SDR-EPR measurements with the band-edge light if the detectable amount of A-centers exist in the sample.³² Moreover, formation of the A-centers requires creation of excess vacancies in Czochralski (Cz) grown silicon that has oxygen concentration $\sim 10^{18} \text{ cm}^{-3}$. The excess vacancy generation requires irradiation of electrons, γ -rays, or ions. However, we used irradiated Fz grown silicon samples having the oxygen concentrations much less than 10^{18} cm^{-3} . Other possibilities are thermal donors NL8 and NL10 that have the orthorhombic symmetry but their g -factors are completely different from the g -factors of P_m spectrum.²⁸ Therefore, we conclude that P_m is a previously unreported paramagnetic recombination center.

In order to estimate the location of P_m -centers, the dependence of the signal intensities on native oxidation time at room temperature in air after hydrogen termination was measured. The results are shown in Fig. 3. It was found that both P_m and P_b signals disappear by removing the oxide film and emerge again after leaving the sample in air at room temperature for a few days. Because P_b -centers are well known to situate in silicon near the silicon/silicon-dioxide interface, P_m -centers that show the same behavior as P_b in Fig. 3 must situate in the region similar to P_b . The angular dependence of the g -factor of P_m revealed clearly that the

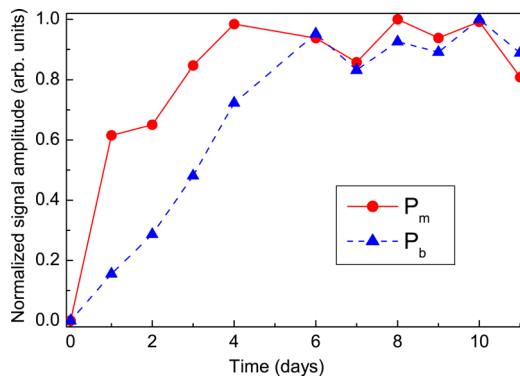


FIG. 3. Time dependences of the SDR-EPR signal intensities detected in the sample kept at room temperature in air after termination of the sample surface by hydrogens. The measurement was performed at $T = 16$ K with $B \parallel [111]$. The signal intensities of P_m (\bullet) and P_b (\blacktriangle) were normalized by the maximum intensities at 8 days and 10 days for P_m and P_b , respectively.

axis of symmetry lies in $\langle 110 \rangle$ direction. If we further imagine that all P_m -centers lie exclusively at the interface of Si/SiO₂, the orthorhombic symmetry can be produced by pairing two neighbor silicon dangling bonds at the interface similar to the A-center formation in the bulk.³⁰ However, further studies are needed to verify such speculations.

From the technological point of view, it is important to investigate whether P_m is detectable after thermal oxidation since it is the standard method to form gate insulators in silicon CMOS transistors. Electron-hole recombination centers like P_m are certainly not welcome at the interface of the gate oxide and channel region. The comparison of SDR-EPR spectra for ²⁸Si sample with native and thermal oxide films (800 °C annealing in O₂ for 1 h) are shown in Fig. 4. Clearly, P_m and I signals are absent, while P_b and P_{b1} signals are seen in the sample with the thermal oxide film. P_{b1} is the defect related to the (100) interface of Si/SiO₂ (Ref. 6). The fact that P_m was not observed here implied that the concentration of P_m by thermal oxidation was less than 10^{11} cm⁻², which is the approximate detection limit of SDR-EPR. Similar spectra with no sign of P_m were also obtained for thermal oxides formed at different temperatures between 800 and

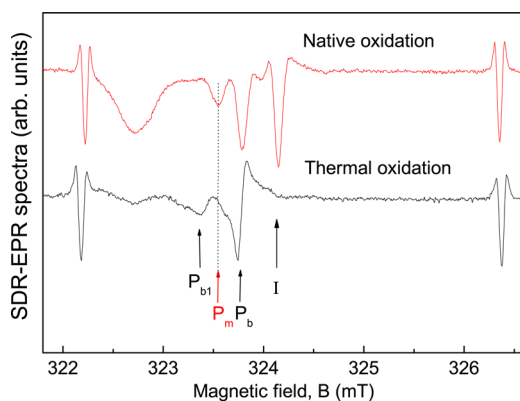


FIG. 4. SDR-EPR spectra of ²⁸Si samples with native and thermal oxide films. The measurements were performed at 16 K with $B \parallel [111]$.

1000 °C. However, it should be stressed here that the absence of P_m line does not mean P_m is irrelevant to the thermal oxides since further optimization of our SDR-EPR measurement may reveal the presence of them.

In summary, we have identified previously unreported P_m -center in the vicinity of silicon/native-dioxide interfaces by electron paramagnetic resonance spectroscopy utilizing spin-dependent-recombination for highly sensitive detection. The P_m -center has the orthorhombic symmetry with $g[110] = 2.0095(2)$, $g[001] = 2.0038(2)$, and $g[\bar{1}10] = 2.0029(2)$.

This work was supported in part by CREST of JST, in part by Grant-in-Aid for Scientific Research and Project for Developing Innovation Systems of MEXT, and in part by Keio G-COE.

¹P. M. Lenahan, and M. A. Jupina, *Colloid. Surf.* **45**, 191 (1990).

²Y. Nishi, *Jpn. J. Appl. Phys., Part 1* **10**, 52 (1971).

³E. H. Poindexter, P. J. Caplan, B. E. Deal, and R. R. Razouk, *J. Appl. Phys.* **52**, 879 (1981).

⁴C. R. Helms and E. H. Poindexter, *Rep. Prog. Phys.* **57**, 791 (1994).

⁵M. Jivanescu, A. Stesmans, and M. Zacharias, *J. Appl. Phys.* **104**, 103518 (2008).

⁶K. Keunen, A. Stesmans, and V. V. Afanas'ev, *Phys. Rev. B* **84**, 085329 (2011).

⁷Y. Nishi, T. Tanaka, and A. Ohwada, *Jpn. J. Appl. Phys., Part 1* **11**, 85 (1972).

⁸A. Stesmans and V. V. Afanas'ev, *J. Appl. Phys.* **83**, 2449 (1998).

⁹P. M. Lenahan and J. F. Conley, *J. Vac. Sci. Technol. B* **16**, 2134 (1998).

¹⁰B. Langhanki, S. Greulich-Weber, and J.-M. Spaeth, *Appl. Phys. Lett.* **78**, 3633 (2001).

¹¹T. D. Mishima and P. M. Lenahan, *IEEE Trans. Nucl. Sci.* **47**, 2249 (2000).

¹²H. J. von Bardeleben, D. Stievenard, A. Grosman, C. Ortega, and J. Siejka, *Phys. Rev. B* **47**, 10899 (1993).

¹³F. Hoehne, J. Lu, A. R. Stegner, M. Stutzmann, M. S. Brandt, M. Rohrmüller, W. G. Schmidt, and U. Gerstmann, *Phys. Rev. Lett.* **106**, 196101 (2011).

¹⁴J. L. Cantin, M. Schoisswohl, and H. J. von Bardeleben, *Phys. Rev. B* **52**, 16 (1995).

¹⁵K. Kato, T. Uda, and K. Terakura, *Phys. Rev. Lett.* **80**, 2000 (1998).

¹⁶A. Stirling, A. Pasquarello, J.-C. Charlier, and R. Car, *Phys. Rev. Lett.* **85**, 2773 (2000).

¹⁷T. Yamasaki, K. Kato, and T. Uda, *Phys. Rev. Lett.* **91**, 146102 (2003).

¹⁸K. Kato, T. Yamasaki, and T. Uda, *Phys. Rev. B* **73**, 073302 (2006).

¹⁹R. L. Vranich, B. Henderson, and M. Pepper, *Appl. Phys. Lett.* **52**, 1161 (1988).

²⁰L. S. Vlasenko, Yu. V. Martynov, T. Gregorkiewicz, and C. A. J. Ammerlaan, *Phys. Rev. B* **52**, 1144 (1995).

²¹R. Laiho, L. S. Vlasenko, and M. P. Vlasenko, *Mater. Sci. Forum* **196**, 517 (1995).

²²L. S. Vlasenko and M. P. Vlasenko, *Mater. Sci. Forum* **196**, 1537 (1995).

²³D. J. Lepine, *Phys. Rev. B* **6**, 436 (1972).

²⁴V. V. Emtsev, Jr., C. A. J. Ammerlaan, A. A. Ezhevskii, and A. V. Gusev, *Physica B* **376**, 45 (2006).

²⁵M. R. Rahman, M. P. Vlasenko, L. S. Vlasenko, E. E. Haller, and K. M. Itoh, *Solid State Commun.* **150**, 2275 (2010).

²⁶A. A. Ezhevskii, A. V. Soukhorukov, D. V. Guseinov, and A. V. Gusev, *Physica B* **404**, 5063 (2009).

²⁷G. Feher, *Phys. Rev.* **114**, 1219 (1959).

²⁸S. H. Muller, M. Sprenger, E. G. Sieverts, and C. A. J. Ammerlaan, *Solid State Commun.* **25**, 987 (1978).

²⁹G. Bemski, *J. Appl. Phys.* **30**, 1195 (1959).

³⁰K. L. Brower, *Phys. Rev. B* **4**, 1968 (1971).

³¹V. Eremin, D. S. Poloskin, E. Verbitskaja, M. P. Vlasenko, L. S. Vlasenko, R. Laiho, and T. O. Niinikoski, *J. Appl. Phys.* **93**, 9659 (2003).

³²R. Laiho, L. S. Vlasenko, M. P. Vlasenko, V. A. Kozlov, and V. V. Kozlovski, *Appl. Phys. Lett.* **74**, 3948 (1999).